

Progress in preparation and applications of Te-As-Se chalcogenide glasses and fibers

Zhihao Wu, Yinsheng Xu, Dongfeng Qi, Qiuhua Nie, Xianghua Zhang

▶ **To cite this version:**

Zhihao Wu, Yinsheng Xu, Dongfeng Qi, Qiuhua Nie, Xianghua Zhang. Progress in preparation and applications of Te-As-Se chalcogenide glasses and fibers. Infrared Physics and Technology, 2019, 102, pp.102981. 10.1016/j.infrared.2019.102981 . hal-02279454

HAL Id: hal-02279454

https://univ-rennes.hal.science/hal-02279454

Submitted on 16 Dec 2019

HAL is a multi-disciplinary open access archive for the deposit and dissemination of scientific research documents, whether they are published or not. The documents may come from teaching and research institutions in France or abroad, or from public or private research centers.

L'archive ouverte pluridisciplinaire **HAL**, est destinée au dépôt et à la diffusion de documents scientifiques de niveau recherche, publiés ou non, émanant des établissements d'enseignement et de recherche français ou étrangers, des laboratoires publics ou privés.

ACCEPTED MANUSCRIPT

Progress in preparation and applications of Te-As-Se chalcogenide glasses and fibers

Zhihao Wu[1,2], Yinsheng Xu[1,3,*], Dongfeng Qi[1,2], Qiuhua Nie[1,2], Xianghua Zhang[3,4]

[1] *Laboratory of Infrared Materials and Devices, Research Institute of Advanced Technologies, Ningbo University, Ningbo, Zhejiang 315211, China*

[2] *Zhejiang Provincial Key Laboratory of Photoelectric Materials and Devices, Ningbo, Zhejiang 315211, China*

[3] *State Key Laboratory of Silicate Materials for Architectures, Wuhan University of Technology, Wuhan 430074, China*

[4] *Laboratory of Glass and Ceramics, UMR CNRS 6226, University of Rennes I, 35042 Rennes Cedex, France*

Abstract: Te-As-Se (TAS) chalcogenide (ChG) glasses are suitable candidates for mid-infrared (MIR) applications. In this work, the formation, preparation of high-purity glasses and optical fibers, and the applications of TAS fibers were systematically reviewed. In this review, the thermal, optical properties as well as the fiber performance parameters of TAS glasses were summarized. Finally, the progress of TAS fibers in MIR applications, especially for sensor applications such as food monitoring and medical diagnostic were described in detail.

Key words: TAS glasses, MIR applications, FEWS, Fiber sensing

ACCEPTED MANUSCRIPT

ACCEPTED MANUSCRIPT

1. Introduction

Chalcogenide (ChG) glasses are composed IVA group elements (S, Se, Te), and added with heavy elements such as Ge, As and Sb, as shown in Fig. 1(a). Compared with traditional silicate glass, ChG glasses have many prominent features including ultra-wide infrared transmission range (up to 25 μm, Fig. 1(b)), lower phonon energy (<350 cm^{-1}), higher linear refractive index n_0 (2.0-3.5) and nonlinear refractive index (100 to 1000 times higher than those of silicate glasses), ultra-fast optical response time (<100 fs), excellent resistance to corrosion in atmospheric environment and tunable composition for different applications[1, 2]. With the above superior performance, ChG glasses have been applied to infrared lens for night vision, phase change memories, electrolytes for batteries, waveguide devices for all-optical signal processing, photoresists for lithography and some new optoelectronic devices[3, 4].

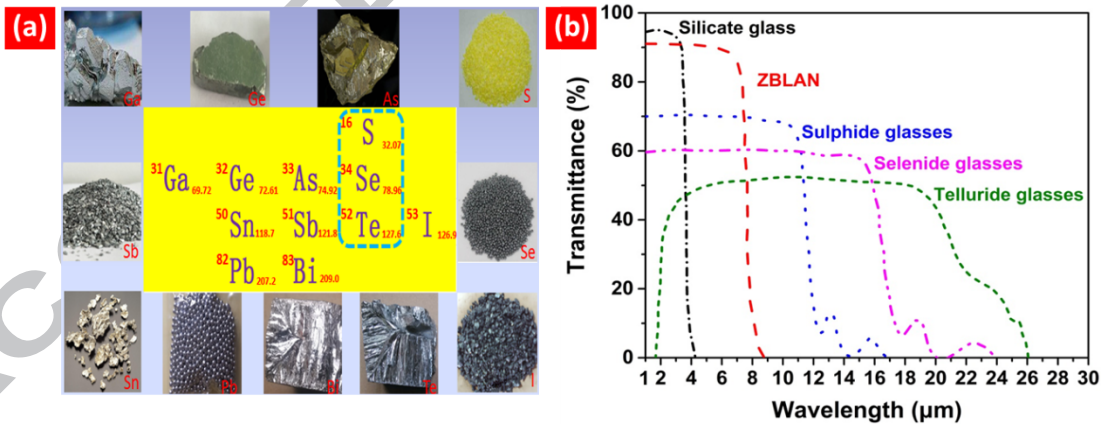


Fig. 1. (a) The commonly used elements for forming chalcogenide glasses and (b) transmission spectra of several glasses.

Besides, ChG glasses are suitable for drawing fibers. ChG fibers have low intrinsic losses, favorable bendability, stable chemical properties, high nonlinear coefficients and ultra-wide infrared transmission range (up to ~26 μm). The ChG fibers have

ACCEPTED MANUSCRIPT

significant applications in the laser delivery[5, 6], transmission of thermal image[7-9], MIR supercontinuum (SC) generation[10-12] and infrared sensing[13-15] since covering the molecular fingerprint region of 3-13 μm MIR bands. To be drawn to a fiber, the glass is required to possess the good thermal stability. Usually, the difference of T_x and T_g larger than 120 °C is the minimum value to avoid crystallization during the drawing process. Until now, ChG fibers such as As-S, As-Se, Ge-As-Se, Ge-Ga-Sb-S (Se), etc are successfully fabricated. Among numerous ChG glasses, TAS glasses have been widely investigated since their excellent thermal stability for drawing fibers and broad transmittance in the MIR[16-18]. TAS fibers have low transmission losses in the 2-18 μm bands, especially in the range of 2-12 μm, which is an ideal medium for detecting fingerprint region molecules [19, 20]. Moreover, TAS fibers have excellent resistance to water, corrosion and electromagnetic interference. They could not only monitor and identify in-situ and long-distance real-time substances in harsh environments such as high temperature (around 100 °C), electromagnetic interference and toxic, but also realize the detection of special aqueous solutions, biological tissues[21], liquids and gaseous substances with infrared characteristic absorption spectra, which has been attracted extensive attention in the fields of biochemistry, microbiology, medical diagnosis, etc[22].

Although TAS glasses have been investigated for half a century, there is no detailed review that summarizes the glass forming, fiber drawing, and applications until now. In this review, we retrospected the formation of TAS glasses first, followed by summary of glass purification technique, the thermal and optical properties of TAS

ACCEPTED MANUSCRIPT

glasses. Finally we introduced the research progress of TAS glasses and fibers in MIR applications and made a prospect.

2. Formation of TAS glasses

2.1 Formation and properties of TAS glasses

In 1976, Kotkata *et al*. first reported the TAS glasses[23]. Generally, ChG glasses were prepared by melt-quenching technique in the vacuumed ampoule ChG glasses [24-26]. As shown in Fig. 2, TAS glass formation domain was relatively large, including As-Se, As-Te, Se-Te binary systems [27, 28]. The As-Se binary system had better glass forming ability than that of As-Te and Se-Te. In the TAS ternary system, the glass forming domain was located in the Se-rich region, which was biased toward the As-Se side.

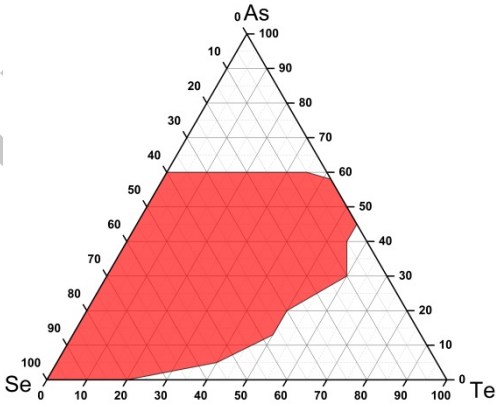


Fig. 2. TAS glasses forming domain. Reprinted with permission from Ref. [27].

Shiryaev *et al*.[29] prepared a series of samples with different Se and Te ratios and systematically studied the effect of $Te_xAs_{40}Se_{60-x}$ (x=0-40, in mol%) compositions on glass forming ability. The differential scanning calorimetry (DSC) of $Te_xAs_{40}Se_{60-x}$ samples at different heating rates were investigated. Fig. 3(a) shows the DSC results with the heating rate of 2.5 K/min. When x= 0, 25, 30, 35, 40, there was an obvious

ACCEPTED MANUSCRIPT

crystallization peak; when x= 5, 10, 15, there was a weak crystallization phenomenon; when x=20, there was no crystallization. When the heating rate was 5 K/min, as shown in Table 1, no crystallization occurred in the compositions of x=10, 15, and 20. When the heating rate was 10 K/min, the x=5, 10, 15, and 20 compositions did not undergo crystallizations as shown in Fig. 3(b). From the formula $K_{gl}= (T_c–T_g)/(T_l–T_c)$ proposed by Hruby[30], we know that the interval $T_c–T_g$ is directly proportional to the glass-forming tendency and the $T_l–T_c$ is indirectly proportional to the glass-forming tendency. Therefore, the TAS glasses of x=5, 10, and 15 compositions were relatively stable. At different heating rates (2.5, 5 and 10 K/min), only $Te_{20}As_{40}Se_{40}$ had no crystallization peak, indicating that this glass was most stable.

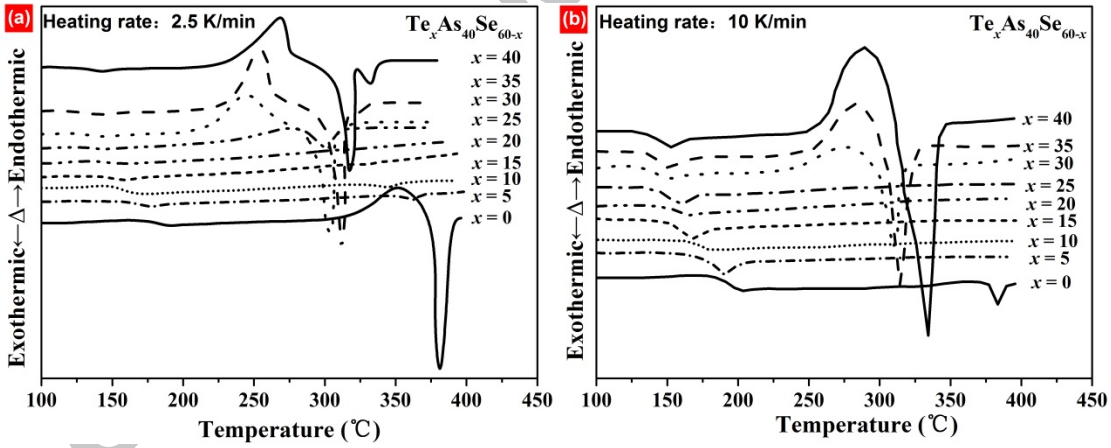


Fig. 3. DSC results for $Te_xAs_{40}Se_{60-x}$ glasses with heating rate of (a) 2.5 K/min, reprinted with permission from Ref. [29] and (b) 10 K/min. Reprinted with permission from Ref. [31].

ACCEPTED MANUSCRIPT

Table 1. Temperature points and criteria of glass stability at heating rate of 5 K/min for $As_{40}Se_{60-x}Te_x$ glasses. Reprinted with permission from Ref. [31].

compositions	T_g/ °C	T_c/ °C	T_p/ °C	T_s/ °C	T_l/ °C	ΔT/ °C	K_{gl}	S/K
$As_{40}Se_{60}$	178	322	356	376	387	145	2.23	10.9
$Te_5As_{40}Se_{55}$	166	306	339	355	368	110	2.26	10.5
$Te_{10}As_{40}Se_{50}$	158	-	-	-	-	-	-	-
$Te_{15}As_{40}Se_{45}$	147	-	-	-	-	-	-	-
$Te_{20}As_{40}Se_{40}$	144	-	-	-	-	-	-	-
$Te_{25}As_{40}Se_{35}$	140	290	309	330	348	150	2.58	6.9
$Te_{30}As_{40}Se_{30}$	130	245	271	297	313	115	1.69	7.4
$Te_{35}As_{40}Se_{25}$	131	244	271	304	327	113	1.36	7.4
$Te_{40}As_{40}Se_{20}$	132	246	277	309	336	114	1.28	8.5

T_g: glass transition temperature, T_c: onset of crystallization temperature, T_p: peak of crystallization temperature, T_s: solidus temperature, T_l: liquidus temperature, $\Delta T=T_c-T_g$, $K_{gl}=(T_c-T_g)/(T_l-T_c)$; $S=(T_p-T_c)(T_c-T_g)/T_g$.

As the DSC results shown, the $Te_{20}As_{40}Se_{40}$ has good thermal stability which has been drawn to fiber. As shown in Fig. 4, the refractive indexes of $Te_{20}As_{40}Se_{40}$ and $Te_{18}As_{40}Se_{42}$ glasses can be close to 3, which was larger than that of silicate glasses. Table 2 shows the mechanical properties and optical windows of the $Te_{20}As_{40}Se_{40}$, TeX and $Ge_{25}Sb_{10}S_{65}$ glasses. TeX glasses, which are built up with Te, Se, and halide elements, show a broad optical transmission in the mid infrared from 2 to about 20 μm, but poor mechanical properties. In contrast, the mechanical behavior of $Ge_{25}Sb_{10}S_{65}$ is improved, but the transmission is limited to 12 μm in the infrared. Between these glasses, TAS glass is an interesting compromise for many applications, with correct mechanical properties and broad-enough transmission range for detection in the molecular fingerprint region.

ACCEPTED MANUSCRIPT

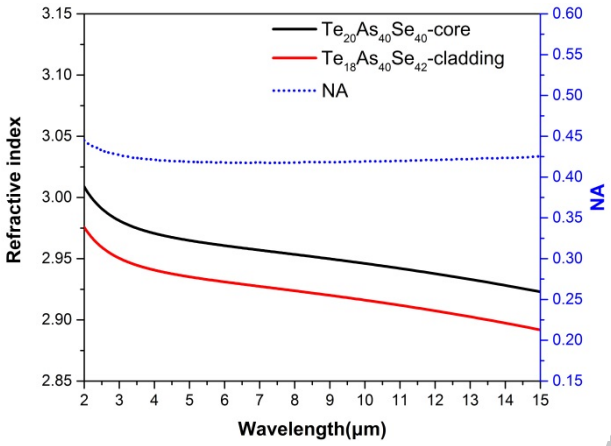


Fig. 4. Refractive indices of fiber core ($Te_{20}As_{40}Se_{40}$) and cladding ($Te_{18}As_{40}Se_{42}$) and the calculated NA. Reprinted with permission from Ref. [18].

Table 2. Young's modulus E, density ρ, linear coefficient of thermal expansion α, micro hardeness H_v, T_g, and optical windows of the $Te_{20}As_{40}Se_{40}$, $Ge_{25}Sb_{10}S_{65}$ and TeX glasses[32] [33].

Glass	E/GPa	ρ/(g·cm^{-3})	α/K^{-1}	H_v/(kg·mm^{-2})	T_g/°C	Optical windows/μm
$Te_{20}As_{40}Se_{40}$	18.0	5.07	23×10^{-6}	146	144	2-16
$Ge_{25}Sb_{10}S_{65}$	18.5	3.4	15.7×10^{-6}	155	320	2-11
TeX glasses	8				60	2-20

2.2 Structure of TAS glasses

Delaizir *et al*. investigated the atomic structure of chalcogenide glasses $As_3Se_{7-x}Te_x$ ($0\leq x\leq3$) and $As_2Se_{3-x}Te_x$ ($0\leq x\leq2.5$) by Wide-Angle X-ray Scattering (WAXS), ^{77}Se NMR as well as Raman and infrared measurements for different compositions[34]. It was shown that the progressive introduction of tellurium in $Te_xAs_3Se_{7-x}$ or $Te_xAs_2Se_{3-x}$ induced breaking of Se-Se bonds and the formation of Te_xAsSe_{3-x} pyramidal units. Experimental data also revealed the absence of Te-Te bonds even in the tellurium richest composition which let suppose a homogeneous repartition of tellurium atoms in the glassy network.

ACCEPTED MANUSCRIPT

Jóvári *et al*. researched the structure of $Te_{20}As_{30}Se_{50}$ glass by X-ray and neutron diffraction as well as extended X-ray absorption fine structure measurements at the As-, Se-, and Te *K*-edges[35]. The five datasets were modelled simultaneously by the reverse Monte Carlo simulation technique. Fig. 5 shows all the chemical bonds in $Te_{20}As_{30}Se_{50}$ glass network, which was a pyramid network structure. Experimental data could be fitted satisfactorily by allowing As-Se, As-Te and Se-Te bonds only. All atoms satisfy the 8-*N* rule (N_{As}=3, N_{Se}=N_{Te}=2) and the affinity of As was much higher to Se than to Te. Chalcogen atoms preferentially bonded to As atom, and Se-Te bonds were formed only after saturating all valences of As.

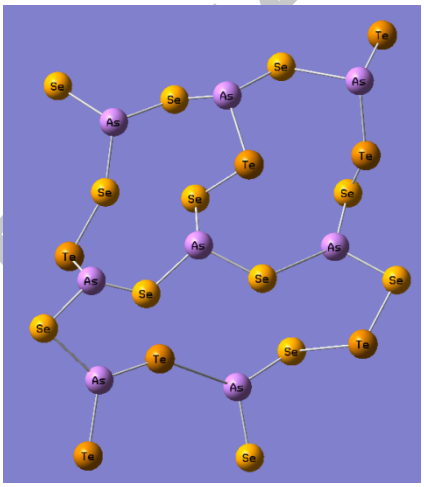


Fig. 5. The atomic structures of $Te_{20}As_{30}Se_{50}$. Reprinted with permission from Ref. [35].

3. Impurity and purification of TAS glasses

The infrared transmission properties of ChG glasses are sensitive to impurities. The impurities in TAS glasses can be divided into two types. The first one is the impurity combined with the glass network or dissolved in the glass matrix. Such impurities usually absorb light selectively. In the fiber loss spectrum, the corresponding

ACCEPTED MANUSCRIPT

absorption peak size is determined by the corresponding impurity concentration, such impurities are mainly combined with H and O. The second one is different from the refractive index of glass, which exhibits scattering of light and then increases the loss of the entire infrared bands including holes, microcrystalline particles and solid inclusions such as SiO_2, carbon, transition metal oxides, etc.

There are three types of impurity sources for TAS glasses [32]. The first category is mainly from raw materials: commercial materials (Te, As, Se) have a purity of 5N (99.999%), thus impurities such as oxygen, molecular water, carbon, and transition metals in the raw materials should be removed as much as possible. Table 3 lists the melting point and purification methods of the raw materials.

Table 3. Melting points, boiling points and purification methods of TAS glasses raw materials.

elements	melting point/ °C	boiling points/ °C	purification methods
Te	450	988	zone melting, distillation invacuum or chemical etching
As	817	615(sublimation)	sublimation in Ar stream or vacuum
Se	217	685	distillation under vacuum, Ar or $SeCl_2$ gas

The second source is from the container for the synthesis of glass at a high temperature. Silica glass tubes are the main container material used for the synthesis of ChG glasses. Hydrogen and silicon dioxide impurities are introduced from the walls of the silica glass tubes. The impurities with high diffusion coefficients, especially hydrogen, can enter the TAS melts easily. It was found that hydrogen started to enter the TAS melts from the silica glass tubes, containing 100 ppm of hydrogen, beginning from 650 °C. The temperature T dependence of a hydrogen

ACCEPTED MANUSCRIPT

entrance rate v ($g \cdot cm^{-2} \cdot s^{-1}$) is described by the expression: $\ln v = -11.2-(15300/T)$, the range of T is 873~1023 K[32]. The chemical interaction of ChG and impurities with silica glass tubes at high temperatures results in the formation of a thin layer on its surface. Owing to the difference in thermo-mechanical properties of the glass matrix and the layers, these layers can be separated from the silica glass tubes and enter the TAS melts to form heterogeneous inclusions, which were represented by α-cristobalite impured with β-cristobalite[32].

The third type of impurity source mainly comes from the reaction of residual gas in the air with TAS glass during vacuuming. Impurities embedded in the glass network include O-H, Se-H, H_2O, As-H as well as N_2, CO_2 and the like. The common impurities in TAS glasses and their corresponding absorption peak wavelengths were described in Ref. [32]. Generally O-H, H_2O, Se-H, and S-H bonds are relatively difficult to remove.

In addition, for the impurities commonly found in the above TAS glasses, impurity mass fraction can be calculated easily according to the Lambert-Beer law, $I=I_0\exp(-\varepsilon xL)$, where I and I_0 are the light fluxes of sample output and input, respectively, ε is the extinction coefficient, x is the impurity mass fraction, and L is the distance (here is the sample thickness). Table 4 shows the extinction coefficients that can be found for some known impurities.

ACCEPTED MANUSCRIPT

Table 4. Extinction coefficients of impurities in TAS glasses. Reprinted with permission from Ref. [32].

Impurities	Extinction coefficient (dB/m)
Se-H	1×10^{-3}
As_2O_3	1.03×10^{-3}
Se-O	3.8×10^{-4}
CO_2	1.5×10^{-2}

For preparing TAS glasses with better performance, the key problem to be solved is to design the purification process to remove the impurities as much as possible. Common oxygen getters such as Al (or Mg) and hydrogen getters such as $TeCl_4$ (or $GaCl_3$, $AlCl_3$) were usually mixed and used together into the raw materials for distillation and purification to synthesize glasses. Table 5 shows the mass fraction of impurities measured by different methods[29]. The addition of $AlCl_3$ can effectively remove hydrogen impurity (about 10 times reduction), and also reduce oxygen and silicon. The carbon mass fraction was almost unchanged, and the mass fraction of metal element impurities was determined by the raw materials and the purification process. Adding an appropriate amount of Al as oxygen getter can effectively reduce the oxygen absorption peak; however this way had a large disadvantage, which would significantly enhance the content of the Se-H peak. It was estimated that the mass fraction of hydrogen could from 0.5 to 4 ppm, when Al exceeds 1 ppm, the molecular H_2O in the glasses network was effectively decomposed. Subsequently the decomposed oxygen and Al formed highly volatile substances, which were removed by distillation, resulting in forming Se-H peak by remaining hydrogen and Se elements.

ACCEPTED MANUSCRIPT

Table 5. Impurity content (ppm wt.) in TAS glasses prepared by different methods.

Reprinted with permission from Ref. [29].

Impurities	Direct synthesis	Melting with Al	Melting with $AlCl_3$
C	1	0.6	1
O	20	0.2	0.6
H	0.2	1	0.02
Si	6	4	0.5
Al	<0.4	<0.5	0.1
Cu	<0.1	<0.1	<0.02
Fe	1	0.8	<0.05
Cr, Ni	<2	<2	<0.03
Mg	0.5	<0.3	<0.01
Sn, Cd	<0.4	<0.5	<0.3
Mn	0.1	<0.1	<0.03
Zn	<0.3	<0.3	<0.2
Pb	<0.5	<0.7	<0.03

To further improve the purity, Hocdé and Shiryaev *et al*. ameliorated the glass preparation technology and obtained high-purity optical fiber preforms. Hocdé *et al*. designed the experimental apparatus as illustrated in Fig. 6[36]. Firstly, the As and Se of 5N purity were heated and evaporated at 290 ℃ and 250 ℃ respectively during the vacuuming process to remove the oxide impurities and molecular water. Subsequently As and Te were introduced into the double chambers tube together with Se. After sealed, the double chambers tube was heated with a temperature gradient furnace designed for melting the elements in the hot zone and then for purification of the melt by distillation into the cold zone. After resealed, the high purity glass was homogenized in a rocking furnace at 700 °C and then cooled down close to the T_g (127 °C). At this temperature, the glass was annealed for several hours and slowly cooled to room temperature. Finally, the high purity TAS glasses were obtained.

ACCEPTED MANUSCRIPT

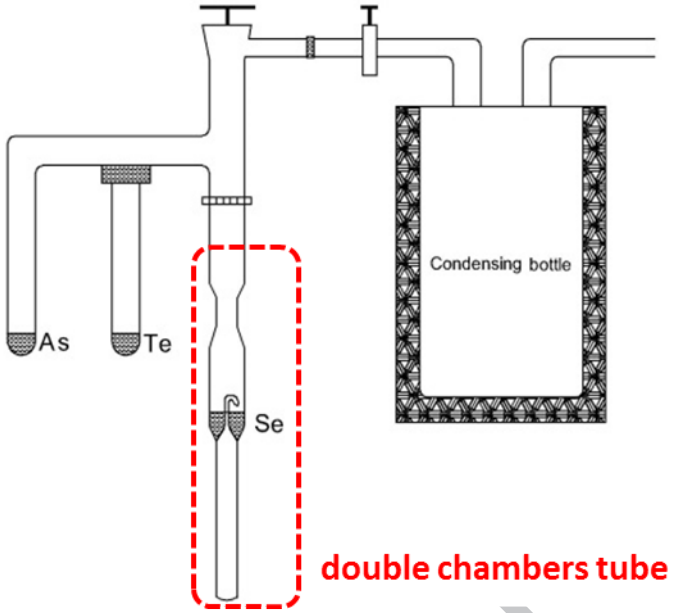


Fig. 6. Experimental set-up used for the purification of the starting elements, Te, As, Se. Reprinted with permission from Ref. [36].

Shiryaev *et al*. studied the distillation purification technology of TAS glasses using the apparatus shown in Fig. 7[20]. First, before using the apparatus, the raw materials As, Se and Te with 5N purity were separately distilled with a low evaporation rate to remove impurities such as oxygen, molecular water, carbon, silicon dioxide and heavy metals. Then 0.07 wt.% of Al as an oxygen scavenger was added in the high-purity raw material after distillation, uniformly mixed and vacuumed. Al_2O_3 was formed in this process to reduce the oxygen-containing components in raw materials. After sealed, the silica tube was placed in a rocking furnace at 850 ^oC for 12 h and cooled to 400 ^oC. Then, it was not necessary to perform quenching and annealing, and the silica tube for melting was directly connected to the double distillation apparatus shown in Fig. 7. The silica tube 1 was filled with Al-containing Te-As-Se glass melt, the silica tube 2 was used as an intermediate transition device, and the silica tube 3 was used for

ACCEPTED MANUSCRIPT

storing the glass melt obtained by the final distillation. The device 5 was silica glass filter, device 6 was a magnetic hammer-breaker used to remove metal impurities which may exist in the vaporized glass melt. The silica tube 1 was first heated to distill the glass melt to the silica tube 2. The boiling point of Al_2O_3 is as high as 2980 ^oC, causing it to remain in silica tube 1 during the subsequent distillation process. Then, the heating temperature of the silica tube 1 was maintained, and the silica tube 2 was heated to condense the glass melt in the silica tube 3. After the second distillation, the silica tube 3 was sealed, melted and homogenized at 700 °C for 7 h. Finally, high purity TAS glasses were obtained by quenching and annealing.

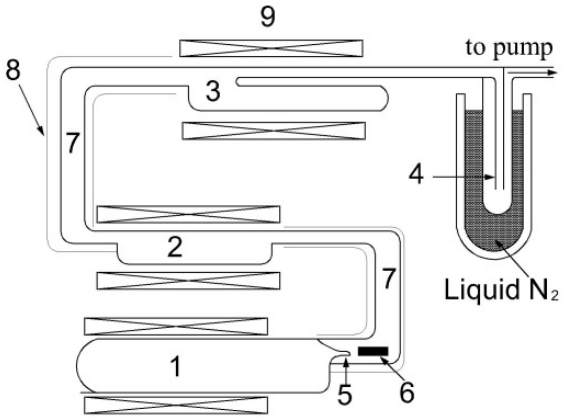


Fig. 7. Set-up for preparing high purity Te-As-Se glasses: 1-silica glass tube with Te-As-Se glass melt after interact with Al getter; 2-intermediate ampoule; 3-synthesis reactor; 4-trap for light volatile impurities; 5-glass partition; 6-magnetic hammer-breaker; 7- silica glass tube; 8-wireheater; 9-furnace. Reprinted with permission from Ref. [20].

4. TAS glasses transmission and fiber loss

The short cut-off wavelength of ChG glasses are caused by electronic transitions,

ACCEPTED MANUSCRIPT

while the IR edge depends mainly on the lattice vibration of the material. The transmission spectrum of the purified glass is shown in Fig. 8(a), especially at 2-12 μm has excellent transmittance[36]. Shiryaev *et al*. added 700 ppm Al to purify the glass preform and drawed the TAS fibers, the lowest losses of the unclad $Te_{25}As_{40}Se_{35}$ and $Te_{20}As_{30}Se_{50}$ fibers were 0.07 dB/m@7.3 μm and 0.04 dB/m@6.7 μm, respectively[20]. In 2006, their group prepared the single mode step-index ($Te_{18.6}As_{39}Se_{42.4}$/$Te_{18.3}As_{39}Se_{42.7}$) glass fiber, the minimum loss was about 0.33 dB/m at 7.5 μm[37]. As shown in Fig. 8(b), the large loss peak in the range of 4-5 μm was mainly due to the influence of Se-H bond, and the loss peak at 6.3 μm was affected by H_2O. Lv *et al*. reduced the C-O peak of the drawn TAS fiber from 1.4 dB/m to 1.1 dB/m by simultaneously improving the TAS glass purification and melting process[38]; the Se-H peak dropped from 1.4 dB/m to 0.9 dB/m; As-O peak decreased from 9.8 dB/m to 6 dB/m.

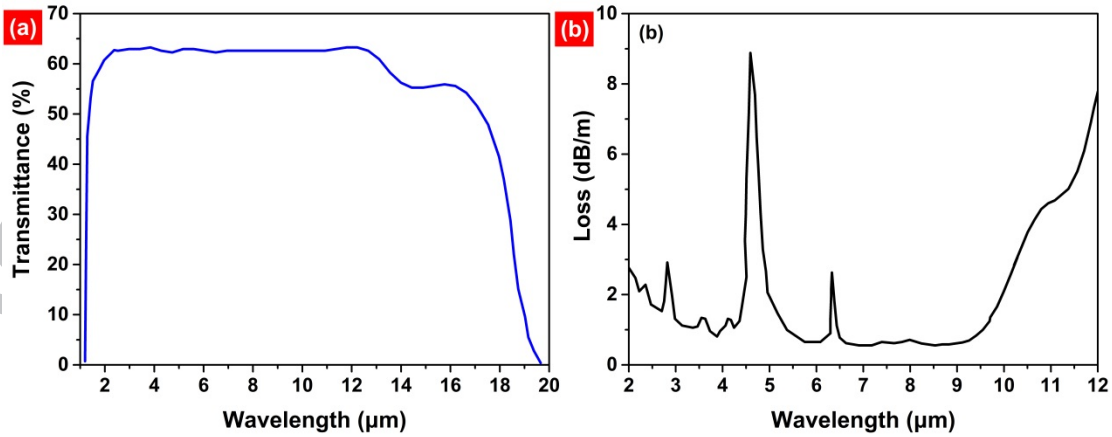


Fig. 8. (a) IR transmission spectrum of the $Te_{20}As_{30}Se_{50}$ glass, reprinted with permission from Ref. [27]; (b)Loss of the $Te_{20}As_{30}Se_{50}$ fiber. Reprinted with permission from Ref. [39].

Recently, our group have new progress in TAS fibers. Fig. 9(a) shows the MIR

ACCEPTED MANUSCRIPT

transmission spectra of $Te_{20}As_{40}Se_{40}$ glass before and after purification. The impurity peaks of the purified glass like O-H, As-O, Se-O, Si-O and H_2O were removed substantially, but the Se-H peak was increased. As shown in Fig. 9(b), the loss remarkably diminished compared after purification, and the unclad $Te_{20}As_{40}Se_{40}$ glass fiber with minimum loss of 1.7 dB/m @ 8.8 μm was obtained.

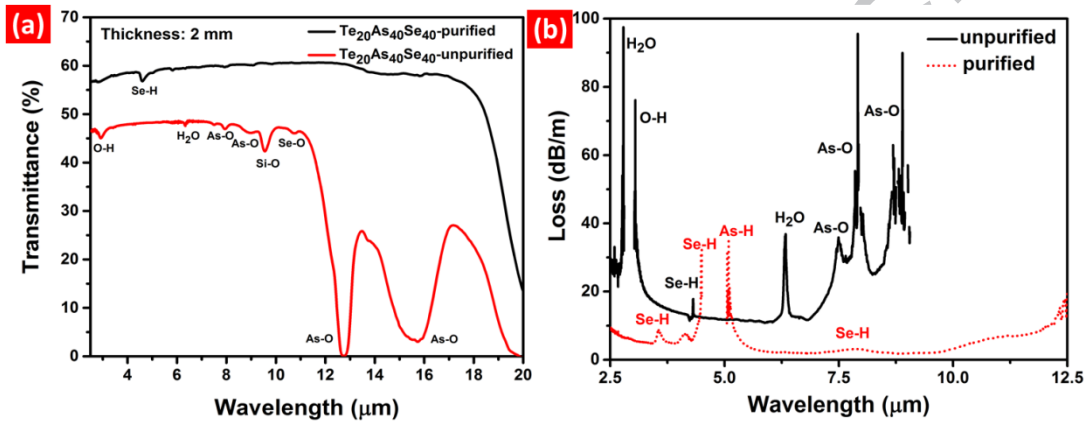


Fig. 9. (a) MIR transmission spectra of $Te_{20}As_{40}Se_{40}$ glass before and after purification and (b) Losses of unclad fibers prepared by using purified and unpurified $Te_{20}As_{40}Se_{40}$ glass. Reprinted with permission from Ref. [18].

Désévédavy *et al.* drew TAS glass into microstructured fiber for the first time[40]. Its cross-sectional view was shown in Fig. 10(a). Single mode transmission could be achieved with a loss of 9 dB/m@3.39 μm and 6 dB/m@9 μm, respectively. The predicted loss is expected to be reduced to 1 dB/m. The fiber loss would be up to 20–30 dB/m when the interstitials holes were collapsed[41]. Fig. 10(b) shows the fundamental mode transmission of 3.39 μm and Gaussian fitting, and the software simulation was basically consistent with the experimental results.

ACCEPTED MANUSCRIPT

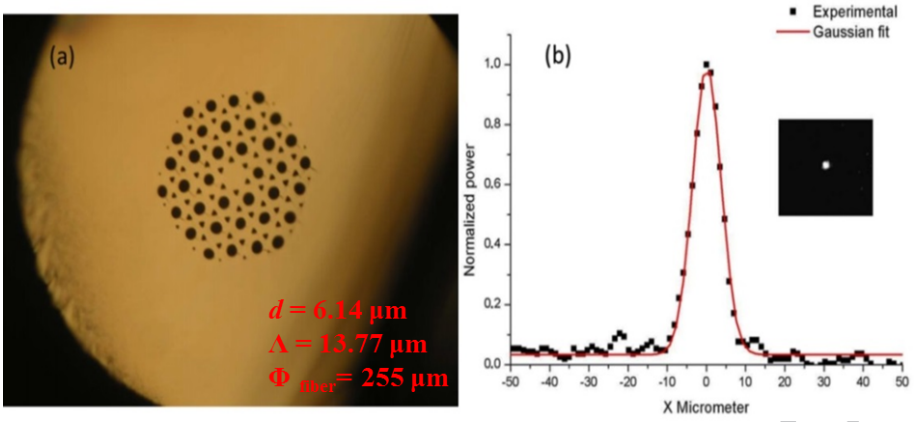


Fig. 10. (a) Microscope image of TAS microstructured fiber, the hole diameter *d* is 6.14 µm and the pitch *Λ* is 13.77 µm (distance between two adjacent hole centers), the outer diameter is 255 µm; (b) Experimental profile of the output beam at 3.39 µm in microstructured TAS fiber together with its Gaussian fit and the inset is a near-field observation of the guided mode at 3.39 µm. Reprinted with permission from Ref. [40].

5. The applications of TAS glasses

5.1 Fiber sensing

The types of fiber sensor mainly include reaction cell light absorption type sensing, sensitive film light reflection and scattering type sensing, fluorescence type sensing, phosphorescence type sensing and evanescent field response type sensing [42]. Currently, TAS fiber sensor is mainly based on the principle of fiber evanescent wave spectroscopy (FEWS), that is, evanescent field response type sensing. Because of the spectral range cover the domain where are located the main IR signatures of molecules and biomolecules, TAS FEWS has been carried out to get some fruitful information in biology and medicine for early stage diagnosis or food safety[43].

According to Snell's law, when the incident angle of light is bigger than the critical

ACCEPTED MANUSCRIPT

angle θ_c, then total internal reflection (TIR) occurs at the interface between the fiber (unclad) and air. The result of interaction with the reflected light is the generation of standing wave near the interface. In general, the phase of the light changes as it is reflected, the amplitude of the standing wave at the interface will be limited. The detailed explanation of Maxwell's equation shows that the standing wave is exponentially attenuated when it extends along the reflection cross section to a medium with a low refractive index, which called evanescent wave. A key parameter is the penetration depth (d_p) of the evanescent field for sensing detection [44].

$$d_p = \frac{\lambda}{2\pi\sqrt{n_1^2 \sin^2\theta - n_2^2}} \quad (1)$$

where λ is the light wavelength, n_2 and n_1 are the refractive indices of the fiber and surrounding detection substance, respectively; θ is the angle of incidence of the wave in the fiber. The penetration of the evanescent wave increases linearly with the wavelength. When the optical fiber is in contact with the liquid to be tested, the infrared light is absorbed by the corresponding characteristic frequency chemical bond to exhibit a characteristic absorption spectrum. According to the absorption spectrum obtained by the contact of the evanescent wave on the surface of the fiber with the substance to be tested, it is extremely possible to detect the chemical substance and concentration, which does not destroy the substance itself and realizes remote sensing[45]. To improve the sensitivity of the FEWS detection and make the evanescent wave be more diffused into the sample, usually, the structure of the optical fiber is modfied. For example, the core-cladding and the tapered fibers as well as the single/multimode fibers combination, fiber bonding and other methods[43]. The

ACCEPTED MANUSCRIPT

FEWS principle of normal fiber and tapered fiber set-up is shown in Fig. 11, respectively. The sensing zone in contact with the sample to be tested generally utilizes the tapered fiber, because the number of total internal reflections in the taper region is significantly increased, resulting that the sensitivity of the sensing can be effectively enhanced [46].

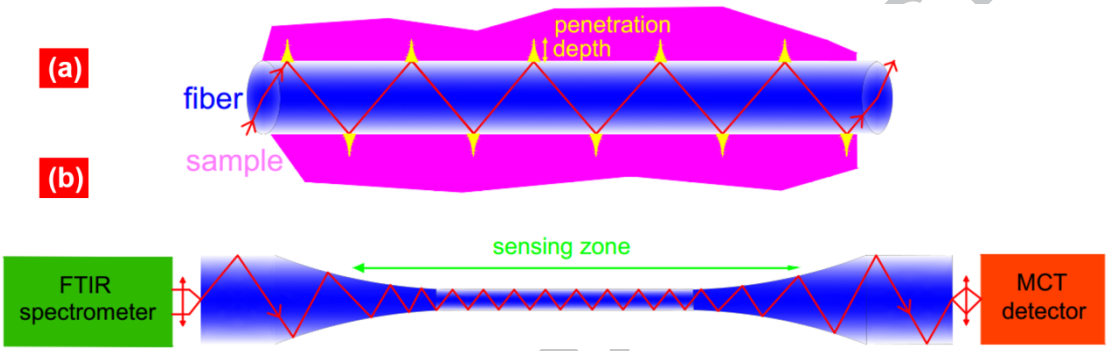


Fig. 11. Principle of FEWS: (a) Normal fiber, (b) Tapered fiber.

TAS fibers have excellent MIR transmission characteristics as well as corrosion resistance and insensitivity to electromagnetic wave. Therefore, researchers have extensive research in the fields of biological and liquid sensing.

TAS fibers in biology detection: Keirsse *et al*. built a TAS fibers sensing set-up composed by a TAS tapered fiber, a Fourier transformed infrared (FTIR) spectrometer and a liquid nitrogen-cooled HgCdTe (MCT) detector. They applied FEWS principle for different condition (hunger and normal) to study mice' liver cells and detected the diseased tissue cells successfully. Bureau *et al*. constructed a experimental set-up as shown in Fig. 12. TAS tapered fibers were both used as transmission and sensing elements. As shown in Fig. 13, the symmetry and asymmetry vibrations of CH_2 groups were successfully detected at 2853 cm^{-1} and 2926 cm^{-1}, respectively. Besides, the symmetrical and asymmetric vibrations of the

ACCEPTED MANUSCRIPT

CH_3 group were successfully detected at 2871 cm^{-1} and 2960 cm^{-1}, respectively. Lucas *et al*. used TAS tapered fiber to place human lung cells with Triton X-100, and successfully detected infrared spectral changes caused by methyl and methylene hydrocarbons in the range of 2800-3000 cm^{-1}, which demonstrated the possibility of the ChG fibers for cell-based biosensors[47]. TAS fiber biosensors, small, simple and sensitive, can monitor various metabolic cells in situ, which can used for early diagnosis of tumors and cancers in medical fields. Therefore, it has extremely inclusive prospects in medicine and microbiology applications[19].

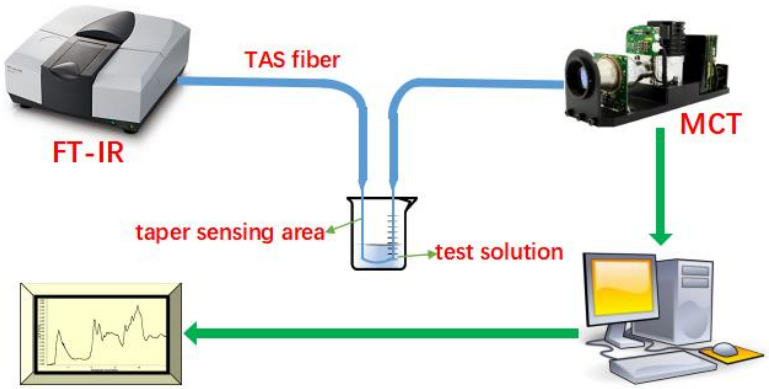


Fig. 12. The monitoring experiment of human lung cell. Reprinted with permission from Ref. [48].

ACCEPTED MANUSCRIPT

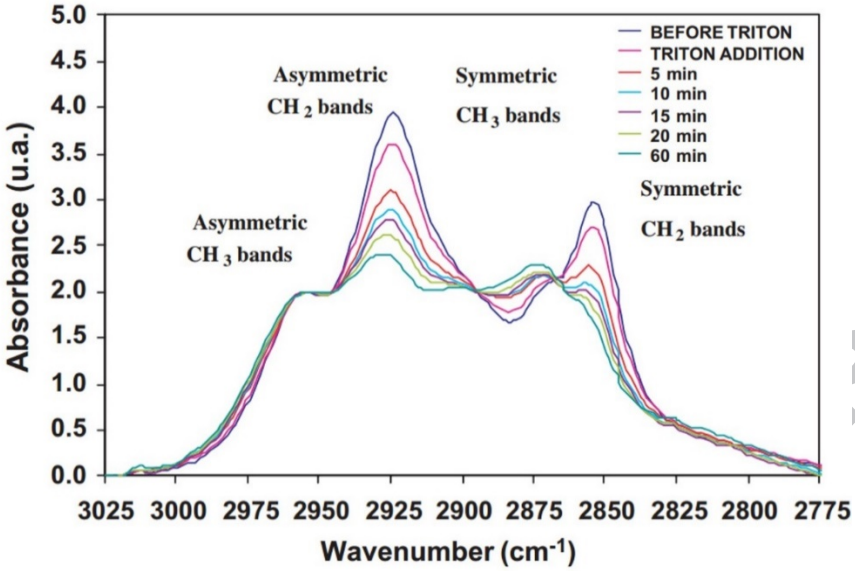


Fig. 13. Infrared spectra of human lung cell recorded with the TAS glass fiber. Reprinted with permission from Ref. [48].

TAS fibers in liquid detection: Hocdé *et al*. used a TAS tapered fiber in a dichloromethane liquid and successfully detected the spectra of acetone (C=O) with different concentration and tracked the C=O absorption spectra as time changed, which is shown in Fig. 14. Michel *et al*. used a 0.2 m long TAS tapered fiber in an artificial water storage system to measure the presence of C_2Cl_4 organic contaminants, finding that the spectrum changed mainly at 908 cm^{-1} shown in Fig. 15. The longer detection time and the higer concentration of the tested liquid, resulting in the more obvious spectral absorption peak; the lowest concentration of the detected pollutant was 1 mg/dm^3 (1 ppm). Besides, they used the TAS tapered fiber protected by special metal and plastic to measure the volatile organic compounds like C_2Cl_4, C_2HCl_3, $C_6H_4Cl_2$, which was in the groundwater of the dustrial lands in Paris and Technical University of Munich. The characteristic peak absorption was detected at the corresponding 1036 cm^{-1}, 1255 cm^{-1}, and 910 cm^{-1} in the IR spectra, respectively, as

ACCEPTED MANUSCRIPT

shown in Fig. 16. TAS fibers can be applied for tracking control and liquid sensing monitoring in chemical reaction processes, effectively improves human's living environment and food quality.

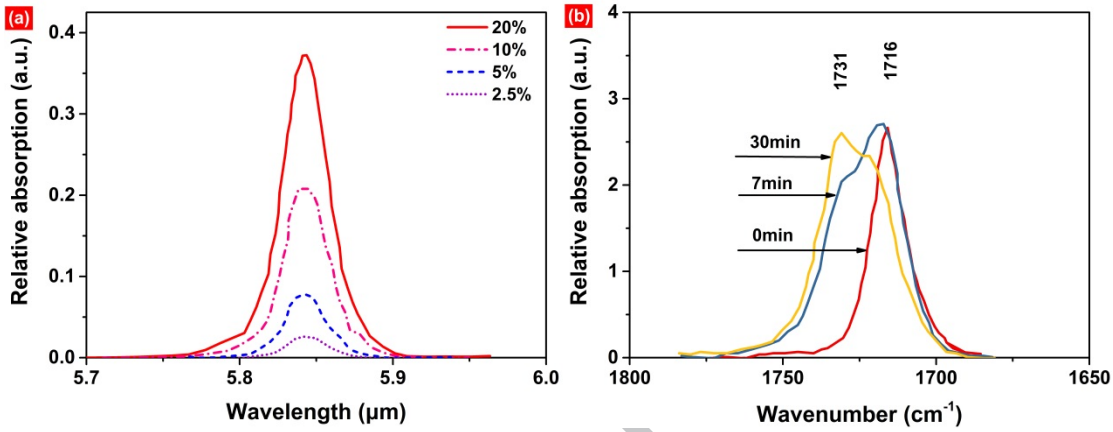


Fig. 14. (a)Detection of C=O band of acetone at different volumic percentages in methylene chloride using FEWS; (b) C=O band shift at different times during microwave assisted organic reaction. The reaction kinetics is followed in situ by FEWS. Reprinted with permission from Ref. [49].

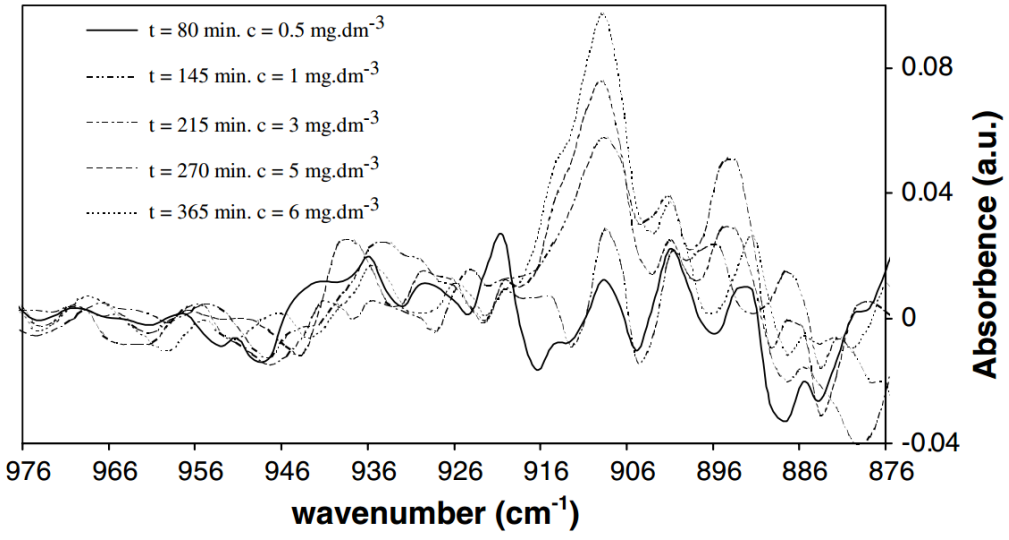


Fig. 15. Evolution of the absorbence of the C_2Cl_4 line at 908 cm^{-1} for a length of immersion of the fiber equal to 0.2 m. Reprinted with permission from Ref. [50].

ACCEPTED MANUSCRIPT

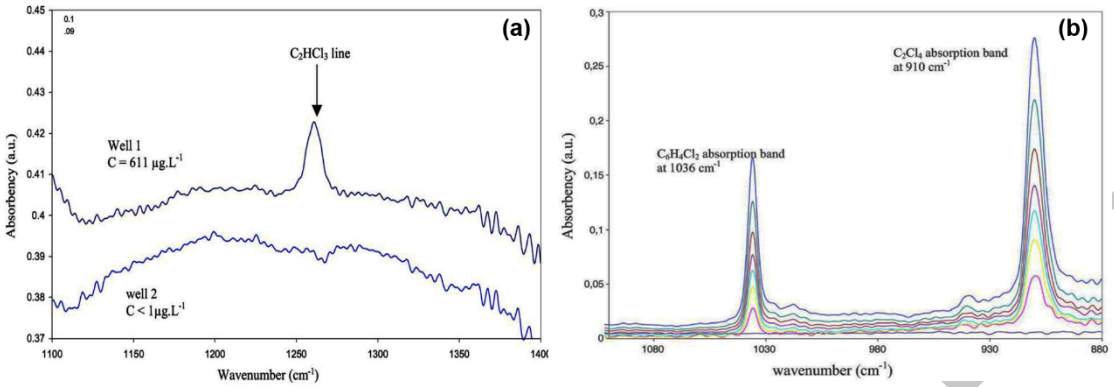


Fig. 16. (a) Spectra recorded near Paris in an industrial fallow land mainly polluted by trichloroethylene (C_2HCl_3). The absorption band of C_2HCl_3 at 1255 cm^{-1} was clearly evidenced for the well 1 and not detectable for the well 2 in agreement with the chemical analysis results; (b) Spectra recorded in Munich in a natural aquifer. It encompassed the both bands of C_2Cl_4 at 910 cm^{-1} and of $C_6H_4Cl_2$ at 1036 cm^{-1} showing that several pollutants can be detected simultaneously. Reprinted with permission from Ref. [39].

The research team in University of Rennes 1 committed to the research of fiber sensing for early disease diagnosis. In June 2011, DIAFIR was founded by an interdisciplinary team of researchers and engineers. Their product, fiber evanescent wave sensor, can be made great use of medical diagnosis shown in Fig. 17. TAS tapered fiber was used to collect information from serum. The system, equipped with an intuitive touch screen interface and a spectrum processing algorithm to directly diagnose the score, only requires a small detection source with 1 mm^2 of tissue or 10 µl of liquid sample (1 drop) [51]. Thanks to timeliness and high sensitivity, it saves hospital stays through invasive and time-consuming surgery and helps doctors get more accurate results and better care for patients. Until now, the non-invasive test has

ACCEPTED MANUSCRIPT

been developed to diagnose the non-alcoholic steato-hepatitis (or NASH) and acute septic arthritis[52, 53].

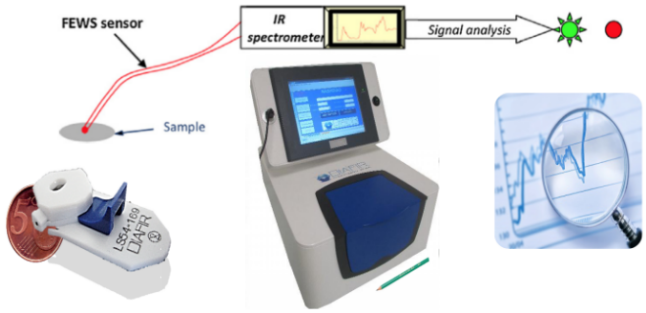


Fig. 17. DIAFIR company's product in France: TAS fiber evanescent wave sensor

5.2 Laser delivery & light propagation

Kosolapav *et al* prepared a TAS microstructured hollow-core fiber shown in Fig. 18, which was firstly demonstrated that it was possible to use the TAS microstructured hollow-core fiber for propagating the 10.6 μm CO_2-laser radiation. A further improvement of the technology and design of such fibers is expected to yield a reduction of the optical loss to below 1 dB/m. This TAS microstructured hollow-core fiber has great promise for the delivery of the CO_2-laser radiation since the light is well limited at the fiber center.

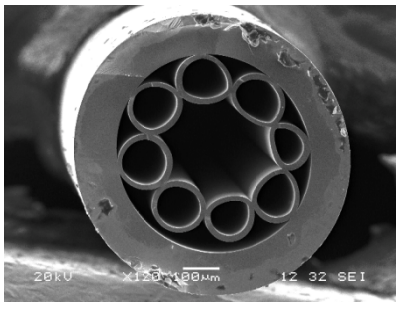


Fig. 18. Fiber cross-section photograph obtained by SEM. Reprinted with permission from Ref. [54].

Houizot *et al*. successfully used the single mode TAS fibers as the wavefront

ACCEPTED MANUSCRIPT

filters to join the DARWIN mission[55], which could successfully detect the the weak infrared emission lines of like O_3 and H_2O on earth-like planets, the scheme as shown in Fig. 19.



Fig. 19. Optical scheme of the detection of the MIR signal coming from an exo-planet through space. The beam profile on the right corresponds to a single-mode TAS glass at 10.6 μm. Reprinted with permission from Ref. [19].

5.3 Supercontinuum generation

The MIR SC generation spectra of ChG fibers, especially the ultra-broadband spectra covering 2–13 μm molecular fingerprint band, are expected to be developed new IR light sources[56, 57]. TAS glasses have high nonlinear refractive index and wide MIR transmission [17], resulting that TAS glasses are more suitable for drawing fibers to obtain ultra-wide spectral conversion than binary sulfur arsenic compounds. Until now, there are few reports on the SC spectra of TAS fibers. Anashkina *et al.* proposed and optimized theoretically a SC laser source in the MIR using Te-As-Se/As-S step-index fiber and pumped by a center wavelength of 150 fs pulse femtosecond all-fiber laser system at 2 μm[58]. Numerically simulated spectra extending from ~1 μm to >8 μm were demonstrated with pumping energy of 100 pJ. Recently, our group have been reported the broadest SC generation spectrum (1.8–13 μm with a 30 dB spectral flatness) by pumping the unclad $Te_{20}As_{40}Se_{40}$ fiber in the normal dispersion region at 5 μm femtosecond laser at different pump powers as

ACCEPTED MANUSCRIPT

shown in Fig. 20(a), which covers almost all the transparent range of the material. By pumping the $Te_{20}As_{40}Se_{40}/Te_{18}As_{40}Se_{42}$ step-index fiber in the normal dispersion region at 5 μm, the SC spectrum covering 2.1–11.2 μm with a 40 dB flatness was recorded(Fig. 20(b))[18].

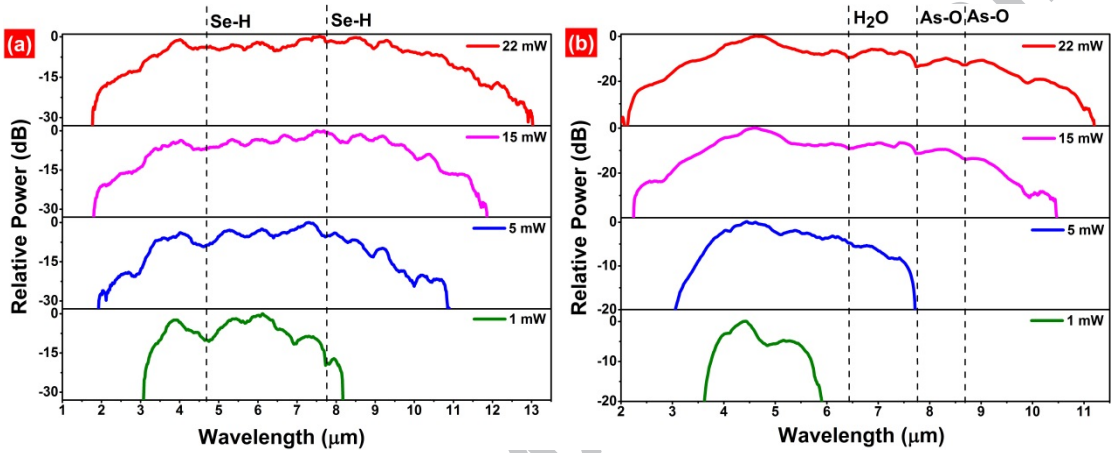


Fig. 20. Spectra of SC at different output power pumped for (a) an unclad $Te_{20}As_{40}Se_{40}$ fiber and (b) a $Te_{20}As_{40}Se_{40}/Te_{18}As_{40}Se_{42}$ step-index fiber. Reprinted with permission from Ref. [18].

6. Conclusion and Prospect

In conclusion, formation of Te-As-Se glasses, their thermal and optical properties, purification technology, the fiber preparation technology, as well as fiber sensing principle and the research progress in sensing applications were reviewed. Although the research of Te-As-Se glasses and fibers have been carried out for nearly half a century, there are still many problems to be solved: firstly, it is necessary to continuously improve the preparation and purification technology to reduce its loss, so as to improve light transmittance and the sensitivity in sensing research. Secondly, the commercial TAS fiber sensors have not appeared except DIAFIR company, therefore, it is necessary to increase its innovation and development with wide range

ACCEPTED MANUSCRIPT

of promotion and application. Finally, there is few TAS fibers report of SC spectrum pupmed by commercial laser, usually, large optical parametric amplifier (OPA) or optical parametric oscillator (OPO) is apply for pumping ChG fibers. Therefore, TAS fiber with proper waveguide dispersion should be designed, such as microstructure and tapered fibers, which makes zero dispersion wavelength blue shift and realize the broadband MIR SC generation.

Acknowledgements

This work was partially supported by the Zhejiang Provincial Natural Science Foundation of China (LY18F050004), Open Research Fund of State Key Laboratory of Transient Optics and Photonics (SKLST201705), National Natural Science Foundation of China (61627815), and K.C. Wong Magna Fund in Ningbo University.

ACCEPTED MANUSCRIPT

ACCEPTED MANUSCRIPT

References

[1] G. Tao, H. Ebendorff-Heidepriem, A.M. Stolyarov, S. Danto, J.V. Badding, Y. Fink, J. Ballato, A.F. Abouraddy, Infrared fibers, Adv. Opt. Photon. 7 (2015) 379-458.

[2] E.A. Anashkina, V.S. Shiryaev, M.Y. Koptev, B.S. Stepanov, S.V. Muravyev, Development of As-Se tapered suspended-core fibers for ultra-broadband mid-IR wavelength conversion, J. Non-Cryst. Solids 480 (2017) 43-50.

[3] J.-L. Adam, X. Zhang, Chalcogenide glasses, Woodhead Publishing, Cambridge, UK, 2014.

[4] L. Lan, H. Lin, S. Qiao, Z. Yi, S. Danto, K. Richardson, J.D. Musgraves, N. Lu, J. Hu, Integrated flexible chalcogenide glass photonic devices, Nat. Photonics 8 (2014) 643-649.

[5] S. Sato, K. Igarashi, M. Taniwaki, K. Tanimoto, Y. Kikuchi, Multihundred-watt CO laser power delivery through chalcogenide glass fibers, Appl. Phys. Lett. 62 (1993) 669-671.

[6] A. Sincore, J. Cook, F. Tan, A. El Halawany, A. Riggins, S. McDaniel, G. Cook, D. Martyshkin, V. Fedorov, S. Mirov, High power single-mode delivery of mid-infrared sources through chalcogenide fiber, Opt. Express 26 (2018) 7313-7323.

[7] H. Suto, Chalcogenide fiber bundle for 3D spectroscopy, Infrared Phys. Technol. 38 (1997) 93-99.

[8] B. Zhang, C. Zhai, S. Qi, W. Guo, Z. Yang, A. Yang, X. Gai, Y. Yu, R. Wang, D. Tang, G. Tao, B. Luther-Davies, High-resolution chalcogenide fiber bundles for

ACCEPTED MANUSCRIPT

infrared imaging, Opt. Lett. 40 (2015) 4384-4387.

[9] S. Qi, B. Zhang, C. Zhai, Y. Li, A. Yang, Y. Yu, D. Tang, Z. Yang, B. Luther-Davies, High-resolution chalcogenide fiber bundles for longwave infrared imaging, Opt. Express 25 (2017) 26160-26165.

[10] C.R. Petersen, U. Møller, I. Kubat, B. Zhou, S. Dupont, J. Ramsay, T. Benson, S. Sujecki, N. Abdel-Moneim, Z. Tang, D. Furniss, A. Seddon, O. Bang, Mid-infrared supercontinuum covering the 1.4–13.3 μm molecular fingerprint region using ultra-high NA chalcogenide step-index fibre, Nat. Photonics 8 (2014) 830-834.

[11] Z. Zhao, B. Wu, X. Wang, Z. Pan, Z. Liu, P. Zhang, X. Shen, Q. Nie, S. Dai, R. Wang, Mid-infrared supercontinuum covering 2.0–16 μm in a low-loss telluride single-mode fiber, Laser Photonics Rev. 11 (2017) 1700005. http://dx.doi.org/10.1002/lpor.201700005

[12] N. Zhang, X. Peng, Y. Wang, S. Dai, Y. Yuan, J. Su, G. Li, P. Zhang, P. Yang, X. Wang, Ultrabroadband and coherent mid-infrared supercontinuum generation in Te-based chalcogenide tapered fiber with all-normal dispersion, Opt. Express 27 (2019) 10311-10319.

[13] R. Chahal, F. Starecki, C. Boussard-Plédel, J.L. Doualan, K. Michel, L. Brilland, A. Braud, P. Camy, B. Bureau, V. Nazabal, Fiber evanescent wave spectroscopy based on IR fluorescent chalcogenide fibers, Sens. Actuators B: Chem. 229 (2016) 209-216.

[14] A.K. Sharma, J. Gupta, R. Basu, Simulation and performance evaluation of fiber optic sensor for detection of hepatic malignancies in human liver tissues, Opt. Laser

ACCEPTED MANUSCRIPT

Technol. 98 (2018) 291-297.

[15] A.P. Velmuzhov, V.S. Shiryaev, M.V. Sukhanov, T.V. Kotereva, M.F. Churbanov, N.S. Zernova, A.D. Plekhovich, Fiber sensor on the basis of $Ge_{26}As_{17}Se_{25}Te_{32}$ glass for FEWS analysis, Opt. Mater. 75 (2018) 525-532.

[16] G. Yang, J.C. Sangleboeuf, C. Boussard-Plédel, B. Bureau, Effect of Physical Aging Conditions on the Mechanical Properties of $Te_2As_3Se_5$ (TAS) Glass Fibers, J. Am. Ceram. Soc. 96 (2013) 464-468.

[17] D. Brandová, R. Svoboda, Thermo-structural characterization of $(As_2Se_3)_{100-x}$-$(As_2Te_3)_x$ glasses for infrared optics, J. Am. Ceram. Soc. 102 (2019) 382-396.

[18] Z. Wu, L. Yang, Y. Xu, P. Zhang, Q. Nie, X. Wang, 1.8–13 μm supercontinuum generation by pumping at normal dispersion regime of As–Se–Te glass fiber, J. Am. Ceram. Soc. https://doi.org/10.1111/jace.16516.

[19] B. Bureau, C. Boussard, S. Cui, R. Chahal, M.-L. Anne, V. Nazabal, O. Sire, O. Loréal, P. Lucas, V. Monbet, Chalcogenide optical fibers for mid-infrared sensing, Opt. Eng. 53 (2014) 027101.

[20] V.S. Shiryaev, J.L. Adam, X.H. Zhang, C. Boussard-Plédel, J. Lucas, M.F. Churbanov, Infrared fibers based on Te–As–Se glass system with low optical losses, J. Non-Cryst. Solids 336 (2004) 113-119.

[21] S. Hocdé, O. Loréal, O. Sire, B. Turlin, C. Boussard-Plédel, D. Le Coq, B. Bureau, G. Fonteneau, C. Pigeon, P. Leroyer, J. Lucas, Biological tissue infrared analysis by chalcogenide glass optical fiber spectroscopy, in: Biomonitoring and

ACCEPTED MANUSCRIPT

Endoscopy Technologies, Porc. SPIE 4158, Amsterdam, Netherlands, 2001, pp. 49-56.

[22] P. Lucas, G.J. Coleman, C. Cantoni, S. Jiang, T. Luo, B. Bureau, C. Boussardpledel, J. Troles, Z. Yang, Chalcogenide glass sensors for bio-molecule detection, in: Optical Fibers and Sensors for Medical Diagnostics and Treatment Applications XVII, Proc. SPIE 10058, San Francisco, California, US, 2017, pp. 100580Q. https://doi.org/10.1117/12.2257995

[23] M.F. Kotkata, S.R. Atalla, M.K. El-Mously, Measurement of the electrical and thermal conductivity coefficients of As_2Se_3-As_2Te_3 glassy alloys, in: G. Klemens, T. K. Chu (Eds.), Thermal Conductivity 14, Springer, US, 1976, pp. 39-44.

[24] Y. Sun, S. Dai, P. Zhang, X. Wang, Y. Xu, Z. Liu, F. Chen, Y. Wu, Y. Zhang, R. Wang, Fabrication and characterization of multimaterial chalcogenide glass fiber tapers with high numerical apertures, Opt. Express 23 (2015) 23472-23483.

[25] M.F. Chubanov, High-purity glasses based on arsenic chalcogenides, Optoelectron. Adv. Mater. 3 (2001) 341-349.

[26] T. Kanamori, Y. Terunuma, S. Takahashi, T. Miyashita, Chalcogenide glass fibers for mid-infrared transmission, J. Lightwave Technol. 2 (1984) 607-613.

[27] B. Bureau, C. Boussard-Pledel, P. Lucas, X. Zhang, J. Lucas, Forming glasses from Se and Te, Molecules 14 (2009) 4337-4350.

[28] Z.U. Borisova, Glassy Semiconductors, Springer US, 1981.

[29] V.S. Shiryaev, M.F. Churbanov, E.M. Dianov, V.G. Plotnichenko, J.L. Adam, J. Lucas, Recent progress in preparation of chalcogenide As-Se-Te glasses with low

ACCEPTED MANUSCRIPT

impurity content, J. Optoelectron. Adv. Mater. 7 (2005) 1773-1779.

[30] A. Hrubý, Evaluation of glass-forming tendency by means of DTA, Czechoslovak Journal of Physics B 22 (1972) 1187-1193.

[31] V.S. Shiryaev, J.L. Adam, X.H. Zhang, M.F. Churbanov, Study of characteristic temperatures and nonisothermal crystallization kinetics in As Se Te glass system, Solid State Sci. 7 (2005) 209-215.

[32] G. Snopatin, V. Shiryaev, V. Plotnichenko, E. Dianov, M. Churbanov, High-purity chalcogenide glasses for fiber optics, Inorg. Mater. 45 (2009) 1439-1460.

[33] J. Lucas, X. Zhang, The tellurium halide glasses, J. Non-Cryst. Solids 125 (1990) 1-16.

[34] G. Delaizir, M. Dussauze, V. Nazabal, P. Lecante, M. Dollé, P. Rozier, E.I. Kamitsos, P. Jovari, B. Bureau, Structural characterizations of As–Se–Te glasses, J. Alloys Compd. 509 (2011) 831-836.

[35] P. Jóvári, B. Bureau, I. Kaban, V. Nazabal, B. Beuneu, U. Rütt, The structure of $As_3Se_5Te_2$ infrared optical glass, J. Alloys Compd. 488 (2009) 39-43.

[36] S. Hocdé, G. Fonteneau, J. Lucas, Chalcogens Based Glasses for IR Fiber Chemical Sensors, Solid State Sci. 3 (2001) 279-284.

[37] V. Shiryaev, C. Boussard-Plédel, P. Houizot, T. Jouan, J.-L. Adam, J. Lucas, Single-mode infrared fibers based on Te-As-Se glass system, Mater. Sci. Eng. B 127 (2006) 138-143.

[38] B. Lv, K. Yang, H. Lang, H. Xue, Effect of trace impurities on loss of As-Se-Te glass infrared fiber, Laser Infra. 31 (2001) 121-123.

ACCEPTED MANUSCRIPT

[39] K. Michel, B. Bureau, C. Boussard-Pledel, T. Jouan, J.L. Adam, K. Staubmann, T. Baumann, Monitoring of pollutant in waste water by infrared spectroscopy using chalcogenide glass optical fibers, Sens. Actuators B: Chem. 101 (2004) 252-259.

[40] F. Désévédavy, G. Renversez, J. Troles, L. Brilland, P. Houizot, Q. Coulombier, F. Smektala, N. Traynor, J.L. Adam, Te-As-Se glass microstructured optical fiber for the middle infrared, Appl. Opt. 48 (2009) 3860-3865.

[41] L. Brilland, J. Troles, P. Houizot, F. Desevedavy, Q. Coulombier, G. Renversez, T. Chartier, T.N. Nguyen, J.-L. Adam, N. Traynor, Interfaces impact on the transmission of chalcogenides photonic crystal fibres, J. Ceram. Soc. Jpn. 116 (2008) 1024-1027.

[42] M. Ramakrishnan, G. Rajan, Y. Semenova, G. Farrell, Overview of fiber optic sensor technologies for strain/temperature sensing applications in composite materials, Sensors 16 (2016) 99.

[43] B. Bureau, C. Boussard, V. Nazabal, J. Troles, Development of chalcogenide glass fibers for mid-IR technologies, in: Smart Photonic and Optoelectronic Integrated Circuits XX, Proc. SPIE 10536, San Francisco, California, United States, 2018, 1053605. https://doi.org/10.1117/12.2288557

[44] X. Jiang, A. Jha, Engineering of a Ge–Te–Se glass fibre evanescent wave spectroscopic (FEWS) mid-IR chemical sensor for the analysis of food and pharmaceutical products, Sens. Actuators B: Chem 206 (2015) 159-169.

[45] S. Cui, R. Chahal, C. Boussard-Plédel, V. Nazabal, J.L. Doualan, J. Troles, J. Lucas, B. Bureau, From selenium-to tellurium-based glass optical fibers for infrared

ACCEPTED MANUSCRIPT

spectroscopies, Molecules 18 (2013) 5373-5388.

[46] X. Jiang, A. Jha, An infrared fibre evanescent wave spectroscopic (FEWS) sensor using purified GeTeSe chalcogenide fibres, in: 20th International Conference on Optical Fibre Sensors, Proc. SPIE 7503, Edinburgh, United Kingdom, 2009, pp. 750319.

[47] P. Lucas, D. Le Coq, C. Juncker, J. Collier, D.E. Boesewetter, C. Boussard-Plédel, B. Bureau, M.R. Riley, Evaluation of toxic agent effects on lung cells by fiber evanescent wave spectroscopy, Appl. Spectrosc. 59 (2005) 1-9.

[48] B. Bureau, X.H. Zhang, F. Smektala, J.L. Adam, J. Troles, H.L. Ma, C. Boussard-Plèdel, J. Lucas, P. Lucas, D. Le Coq, Recent advances in chalcogenide glasses, J. Non-Cryst. Solids 345-346 (2004) 276-283.

[49] S. Hocdé, C. Boussard-Plédel, G. Fonteneau, D. Le Coq, H.L. Ma, J. Lucas, Recent developments in chemical sensing using infrared glass fibers, J. Non-Cryst. Solids 274 (2000) 17-22.

[50] K. Michel, B. Bureau, C. Pouvreau, J.C. Sangleboeuf, C. Boussard-Plédel, T. Jouan, T. Rouxel, J.-L. Adam, K. Staubmann, H. Steinner, T. Baumann, A. Katzir, J. Bayona, W. Konz, Development of a chalcogenide glass fiber device for in situ pollutant detection, J. Non-Cryst. Solids 326–327 (2003) 434-438.

[51] M.L. Corvec, F. Charpentier, A. Kachenoura, S. Bensaid, S. Henno, E. Bardou-Jacquet, B. Turlin, V. Monbet, L. Senhadji, O. Loréal, Fast and non-invasive medical diagnostic using mid infrared sensor: The AMNIFIR project, IRBM 37 (2016) 116-123.

ACCEPTED MANUSCRIPT

[52] R. Anty, M. Le Corvec, A. Iannelli, S. Patouraux, M.-C. Saint-Paul, A.-S. Schneck, C. Canivet, I. Ben-Amor, J. Gugenheim, O. Sire, Mid-infrared spectroscopy has a high sensitivity and specificity for point-of-care diagnosis of non-alcoholic steato-hepatitis, J. Hepato. 64 (2016) S177.

[53] J.-D. Albert, V. Monbet, A. Jolivet-Gougeon, N. Fatih, M. Le Corvec, M. Seck, F. Charpentier, G. Coiffier, C. Boussard-Plédel, B. Bureau, A novel method for a fast diagnosis of septic arthritis using mid infrared and deported spectroscopy, Joint Bone Spine 83 (2016) 318-323.

[54] A.F. Kosolapov, A.D. Pryamikov, M.S. Astapovich, V.S. Shiryaev, G.E. Snopatin, V.G. Plotnichenko, A.S. Biriukov, M.F. Churbanov, E.M. Dianov, Demonstration of waveguide regime for chalcogenide hollow-core optical fiber with negative curvature of core boundary from mid- to far-infrared, in: 2011 Conference on Lasers and Electro-Optics Europe and 12th European Quantum Electronics Conference (CLEO EUROPE/EQEC), IEEE, Munich, Germany, 2011.

[55] A.J. Faber, B. Bureau, C. Boussardplédel, J. Lucas, J.P.D. Carmo, L.K. Cheng, P. Houizot, P.A.V. Nijnatten, W.L.M. Gielesen, Infrared single mode chalcogenide glass fiber for space, Opt. Express 15 (2007) 12529-12538.

[56] P. Cimalla, J. Walther, M. Mittasch, E. Koch, Shear flow-induced optical inhomogeneity of blood assessed in vivo and in vitro by spectral domain optical coherence tomography in the 1.3 μm wavelength range, J. Biomed. Opt. 16 (2011) 116020.

[57] C.R. Petersen, N. Prtljaga, M. Farries, J. Ward, B. Napier, G.R. Lloyd, J. Nallala,

ACCEPTED MANUSCRIPT

N. Stone, O. Bang, Mid-infrared multispectral tissue imaging using a chalcogenide fiber supercontinuum source, Opt. Lett. 43 (2018) 999-1002.

[58] E.A. Anashkina, V.S. Shiryaev, G.E. Snopatin, S.V. Muraviev, A.V. Kim, On the possibility of mid-IR supercontinuum generation in As-Se-Te/As-S core/clad fibers with all-fiber femtosecond pump source, J. Non-Cryst. Solids 480 (2017) 38-42.

- Formation and properties of Te-As-Se glasses were reviewed.
- Applications in optics and medical of Te-As-Se fibers were summarized.
- Prospects of the applications in medical diagnosis and supercontinuum generation.

Declarations of interest: none

ACCEPTED MANUSCRIPT